Journal of Materials Chemistry C

ROYAL SOCIETY OF CHEMISTRY

PAPER

View Article Online
View Journal | View Issue

Cite this: J. Mater. Chem. C, 2022, 10, 6770

Strain enhancement due to oxygen vacancies in perovskite oxide films†

M. Tyunina, *[ab] J. Levoska,[a] O. Pacherova,[b] T. Kocourek[b] and A. Dejneka[b]

Received 15th October 2021,
Accepted 31st March 2022

DOI: 10.1039/d1tc04969k

rsc.li/materials-c

Control of lattice strain in epitaxial films of ABO_3 perovskite oxides is crucial for modern understanding and applications of these scientifically and technologically important materials. Here, we show that oxygen vacancies have unique impacts on lattice strain in such films. We suggest that in the presence of substrate-imposed misfit in epitaxial or highly oriented films, the crystallographic alignment of anisotropic elastic dipole tensors of oxygen vacancies is energetically favorable. The dipolar alignment leads to an enhanced above-misfit magnitude of maximal lattice strain and to increased inhomogeneous strain or strain gradients. The vacancy-induced remarkably strong elastic effects are experimentally validated by varying the misfit strain and oxygen content in thin films of perovskite niobate ($ANbO_3$) and titanate ($ATiO_3$) ferroelectrics. It is anticipated that elastic effects of oxygen vacancies are relevant for controlling strain in epitaxial films of a broad range of functional oxides.

Introduction

Numerous ABO_3-type perovskite metal oxides exhibit substantial functional responses to external stimuli, demonstrate a variety of strong effects, possess diverse electronic properties, and host remarkable ordering phenomena. Ferroelectrics, multiferroics, and high-temperature superconductors are just a few examples of these scientifically intriguing and technologically important multifunctional materials. Whereas relevant applications of many of these materials have been established, extensive efforts have been made to understand the fundamentals of perovskites and to develop advanced oxides for emerging innovations.

An essential new research field has arisen due to progress in synthesizing epitaxial ABO_3 films.[1,2] Beyond being in demand for basic studies and integrated devices, epitaxial films enable unusual phenomena that stem from couplings between a film and an underlying substrate. In particular, because of elastic coupling, a film-substrate mismatch in lattice parameters, symmetries, and/or thermal expansion coefficients imposes a lattice strain, which leads to unprecedented crystal phases and unparalleled properties of epitaxial films.[3–9] Furthermore, the epitaxial growth of a film experiencing a substrate-imposed misfit strain is regulated by elastic energy that increases with increasing film thickness.[10] There is a certain critical thickness at which strain relaxation starts. For many perovskite oxides, the critical thickness is a few to a few tens of nanometers at a magnitude of misfit strain from 2 to 1%. Notably, the relaxation of misfit strain generates a distribution of strain across the thickness of the film and, accordingly, leads to out-of-plane strain gradients.[11] The presence of such inhomogeneous strains has an abundance of implications for film properties.[12–16] Overall, it is imperative for research and innovations to precisely control the lattice strain, strain gradients, and critical thickness in perovskite oxide films.

Basically, the phase stability and phenomenal behavior of ABO_3 perovskites are fundamentally related to oxygen sites, which comprise 60% of all atoms therein. Concurrently, oxygen vacancies are the most frequent point defects in these materials. Whereas point defects in solids are generally known to possess specific elastic properties, the elastic properties and interactions of oxygen vacancies in perovskite oxides are poorly studied and mostly disregarded for strained epitaxial films. This work addresses the unique epitaxial effects that arise due to elastic interactions of oxygen vacancies with film-substrate misfit strain in perovskite oxide films.

Here, we first qualitatively show that misfit strain can promote specific crystallographic alignment of anisotropic elastic dipoles of oxygen vacancies. This alignment, in turn, can significantly affect the growth and structure of the films. We suggest that the alignment can raise the critical thickness, lead to a profound enlargement of the lattice strain above the theoretical misfit magnitude and produce a substantial inhomogeneous strain. Next, we demonstrate experimental verification and reproducibility of these effects using epitaxial films

[a] Microelectronics Research Unit, Faculty of Information Technology and Electrical Engineering, University of Oulu, P. O. Box 4500, FI-90014 Oulu, Finland. E-mail: marina.tjunina@oulu.fi
[b] Institute of Physics of the Czech Academy of Sciences, Na Slovance 2, 18221 Prague, Czech Republic

† Electronic supplementary information (ESI) available. See https://doi.org/10.1039/d1tc04969k

of perovskite ferroelectric niobates and titanates. The films were grown on compressive substrates, and oxygen vacancies were introduced therein *in situ*, during the growth. Finally, we briefly discuss the potential implications and further studies of the demonstrated effects.

Methods

Thin (~100 nm) films of $NaNbO_3$ (NNO), $K_{0.5}Na_{0.5}NbO_3$ (KNNO), and $Ba_{0.5}Sr_{0.5}TiO_3$ (BSTO) were grown by pulsed laser deposition using an excimer KrF laser (wavelength 248 nm, pulse duration 20 ns, repetition rate 5 Hz). Dense ceramic targets were synthesized at the Institute of Solid State Physics, University of Latvia. During deposition, the target-to-substrate distance was 35 mm, and the area of the irradiated spot and energy density on the target surface were 3 mm^2 and 2 J cm^{-2}, respectively. Mechanical scanning included rotation, precession, and translation of the target and the substrate holder. A substrate temperature of 973 K was kept during deposition and lowered at a rate of 5 K min^{-1} during post-deposition cooling. As an ambient gas, optically pure (99.995%) oxygen was used. The oxygen pressure was kept constant during deposition and post-deposition cooling, and varied from 0.1 Pa to 20 Pa for different samples. The thickness of the films was regulated by number of laser pulses. Epitaxially polished (001)-cut $SrTiO_3$ (STO) and $(La_{0.3}Sr_{0.7})(Al_{0.65}Ta_{0.35})O_3$ (LSAT) substrates were purchased from MTI Corp.

The crystal structure of the films was studied by high-resolution X-ray diffraction (XRD) on a D8 DISCOVER diffractometer (Bruker corporation) using Cu Kα radiation. Θ–2Θ scans in the range of 2Θ = (10–130) deg and reciprocal space maps in the vicinity of the perovskite (002) and (303) diffractions were acquired. The thickness of the films was determined by X-ray reflectometry on the diffractometer. The reflectometry data were fitted using LEPTOS software.

Results and discussion

Elastic effects of oxygen vacancy dipoles

First, we qualitatively consider a general picture of oxygen vacancies in ABO_3 perovskites. Because of the crystal structure of these materials, the formation of an oxygen vacancy (V_O) therein is basically associated with strong anisotropic lattice distortions.[17–26] The distortions lead to the emergence of stress around the vacancy. In elasticity theory, this is described by an elastic dipole tensor.

The dominating primary distortion is a shift of the nearest to vacancy B-cations away from the vacancy along the B–O–B–O-direction and, hence, an elongation of the B–Vo–B distance compared to the B–O–B distance [Fig. 1(a)].[17–26] Consequently, an elastic dipole tensor (or elastic dipole) of the vacancy is anisotropic. It can be approximated by a second rank tensor p_{ij} with nonzero diagonal components, where the main component $D_1 > 0$ is along the B–V_O–B direction and $D_2 = D_3 < 0$ ($D_1 > |D_2|$ or $D_1 \gg |D_2|$) are in the directions orthogonal to the B–V_O–B direction.[27] The anisotropic dipole of oxygen vacancies contrasts with isotropic dipoles of cationic vacancies (V_A or V_B).[27] Additionally, oxygen-cation divacancies (V_A–V_O or V_B–V_O) may possess anisotropic dipoles, but their occurrence is less frequent than V_O and omitted for simplicity.

In a typical cube-on-cube epitaxial perovskite film on a cubic substrate, there is a substrate-imposed biaxial in-plane misfit strain s_a. The corresponding in-plane stress produces an out-of-plane strain s_c: $s_c = -2(c_{12}/c_{11})\cdot s_a$, where c_{11} and c_{12} are the elastic constants of the film's material. Elastic dipoles of oxygen vacancies can interact with external strain s_{ij}, and the energy of this interaction is $E = -p_{ij}s_{ij}$.[28]

Peculiar for cube-on-cube oriented ABO_3 perovskite films, oxygen vacancies can be located in two distinct types of atomic planes parallel to the substrate surface: the [AO] planes (vacancy V_{OA}) and the [BO_2] planes (vacancy V_{OB}) [Fig. 1(a)]. The main elastic component D_1 is along the out-of-plane direction for the V_{OA} vacancy and along either of the in-plane directions for the V_{OB} vacancy. Correspondingly, there are different energies of the vacancy-strain interactions for different locations of the vacancies. For $D_1 \gg |D_2|$, the strain-vacancy interaction energy E_A for the vacancy V_{OA} is approximately [$E_A \approx -2(c_{12}/c_{11})\cdot D_1\cdot s_a$]. The energy E_A dramatically differs from the energy E_B for the vacancy V_{OB}: [$E_A \approx -D_1\cdot s_a$].

These simplified energy considerations show that a compressive misfit $s_a < 0$ favors out-of-plane oriented elastic dipoles, for which $E_A < 0$ and $E_B > 0$. Hence, the V_{OA} vacancies

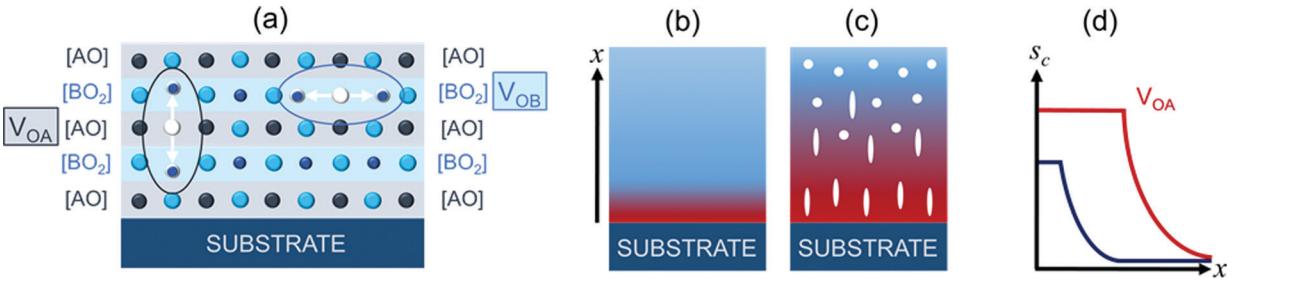

Fig. 1 (a) Schematics of exaggerated displacements of B-cations around oxygen vacancies in different atomic planes. (b and c) Schematics of misfit-strained (b) stoichiometric and (c) oxygen-deficient films on compressive substrates. Strain is shown in red color. In (c), elongated ellipses illustrate out-of-plane aligned dipoles, and circles show random dipoles. (d) Schematics of distribution of the out-of-plane strain across film thickness, $s_c(x)$, for the stoichiometric film in (b) (blue lower curve) and oxygen-deficient film in (c) (red upper curve).

are promoted. Likewise, a tensile misfit $s_a > 0$ facilitates in-plane oriented elastic dipoles, for which $E_A > 0$ and $E_B < 0$. Then the V_{OB} vacancies are fostered. We note that a shift of the B-cations towards the vacancy is also possible.[26] Then the signs of the components of anisotropic elastic dipole tensor change, correspondingly: $D_1 < 0$ and $D_2 = D_3 > 0$. For such B-shifts, a compressive (tensile) misfit can facilitate in-plane (out-of-plane) oriented dipoles and the V_{OB} (V_{OA}) vacancies. In any case, it is anisotropy of the elastic dipole tensor that drives the preferential crystallographic alignment of the dipoles in the presence of misfit strain.

Interestingly, the theoretical *ab initio* calculated formation energies might vary by ~10% for the vacancies in different atomic planes.[19,21,23] In contrast, elastic energies E_A and E_B have opposite signs and thus differ essentially. This elastic-energy difference dominates and likely determines the preferable formation of either V_{OA} or V_{OB} vacancies in the presence of strain in epitaxial films.

In strained epitaxial films, the density W_s (per unit volume) of elastic energy associated with misfit strain is proportional to the strain squared and is always positive: [$W_s \propto (s_a)^2$].[10] For the misfit-aligned elastic dipoles, the energy density W_{VO} of the misfit-vacancy interactions can be approximated as [$W_{VO} \propto EN$]. Here the energy E corresponds to either E_A or E_B and N is the concentration of the aligned dipoles. For the favorable dipolar orientation, the density W_{VO} is negative. Thus, the misfit-stimulated formation of specific V_{OA} or V_{OB} vacancies and related definite crystallographic alignment of the vacancy dipoles diminishes the total density of elastic energy in the film.

Ideally, in the presence of a sufficient concentration of oxygen vacancies, the favorable dipolar alignment can fully compensate for misfit energy: $W_{VO} = -W_s$. Then the coherent growth of an infinitely thick strained film is enabled. Generally, for a certain vacancy concentration, the critical thickness d_{VO} for strain relaxation in an oxygen-deficient film [Fig. 1(b)] can exceed the critical thickness d_O in a vacancy-free film [Fig. 1(c)] owing to the dipolar alignment. Thus, the presence of oxygen vacancies and the misfit-stimulated alignment of the vacancy dipoles can raise the critical thickness.

Another effect of aligned vacancy dipoles is an anisotropic chemical strain s_{chem}. For instance, a compressive in-plane misfit strain [$s_a < 0$] enforces the corresponding out-of-plane orientation of the vacancy dipoles, each of which is characterized by a local lattice elongation (along D_1). The out-of-plane oriented dipoles produce a tensile out-of-plane strain in a chemically expanded unstressed material of the film, which can be approximated as [$s_{chem} \approx ND_1/c_{11}$].[28] Accordingly, the resulting magnitude of the out-of-plane strain in the oxygen-deficient film can substantially exceed that of the purely substrate-determined misfit strain s_c in the stoichiometric film [Fig. 1(d)]. Such vacancy-induced anisotropic chemical strains are peculiar for heteroepitaxial or highly oriented films. In bulk crystals, the vacancy dipoles are randomly oriented and averaged, which results in a small isotropic chemical strain.[27,29] The presence of misfit strain facilitates the formation of either V_{OA} or V_{OB} vacancies during film growth, producing aligned dipoles and, consequently, anisotropic chemical strain.

In addition to its effects on the critical thickness and maximal strain, dipolar alignment can enhance inhomogeneous strain. In a vacancy-free film, the relaxation of misfit strain leads to a distribution of strain across the film thickness. The strain is maximal (within the critical thickness) in the vicinity of the film-substrate boundary and decreases with distance x from the boundary in the out-of-plane direction. In the presence of oxygen vacancies, the concentration N of the aligned dipoles grows with $|s_a|$ to reduce the total elastic energy. A distribution $s_a(x)$ determines a distribution $N(x)$, which, in turn, imposes a distribution of the chemical strain, $s_{chem}(x)$. Thus, the total inhomogeneous strain can be intensified by the dipolar alignment.

We note that the concentration N of the aligned oxygen vacancy dipoles is upper-limited by the concentration of oxygen vacancies and depends on misfit strain. Generally, both aligned and random dipoles can coexist. Therefore, the type of structural behavior – a peculiar behavior due to aligned dipoles or a conventional behavior – is dictated by strain.

Although the presented considerations are simplified and qualitative, they indicate that elastic interactions of oxygen vacancy dipoles with misfit strain can promote a specific crystallographic alignment of the vacancy dipoles in epitaxial perovskite oxide films. Compared to vacancy-free films, the dipolar alignment can lead to enlarged critical thickness, enhanced above-misfit anisotropic strain, and augmented inhomogeneous strain. Next, we deliver experimental proof for the suggested effects using heteroepitaxial films of perovskite niobates ($ANbO_3$) and titanates ($ATiO_3$). We show similar effects for different types of B-site cations, pointing to a universal character of the vacancy-induced phenomena.

Above-misfit strain in NNO/LSAT films

Hitherto, we investigated lattice strain in thin NNO films grown on LSAT substrates. The theoretical biaxial in-plane misfit strain is compressive [$s_a \approx -1.3\%$] at the growth temperature in a cubic NNO on LSAT. This misfit magnitude suggests a critical thickness for strain relaxation being not larger than 40–50 nm.[30] For the high-temperature cubic phase, the elastic constants are c_{11} = 230 GPa and c_{12} = 90 GPa,[31] and the theoretical out-of-plane strain is tensile [$s_c \approx 1.0\%$] during film growth. The theoretical room-temperature in-plane misfit is [$s_a \approx -0.9\%$] for a low-temperature pseudocubic phase of NNO. Using the model constants $c_{11} \approx 400$ GPa and $c_{12} \approx 70$ GPa,[32] the corresponding out-of-plane tensile strain is estimated as [$s_c \approx 0.3\%$]. Taking into account possible tilts of oxygen octahedra in NNO, the related constants are $c_{11} \approx 170$ GPa and $c_{12} \approx 70$ GPa,[32] and the room-temperature strain may be up to [$s_c \approx 0.7\%$].

Based on the room-temperature XRD inspections [ESI† Fig. S1–S3], the crystal structure of all NNO films can be interpreted as pseudocubic perovskite. The films are epitaxial and highly oriented, with the (00*l*) planes parallel to the substrate (001) surface and with the [100] directions parallel

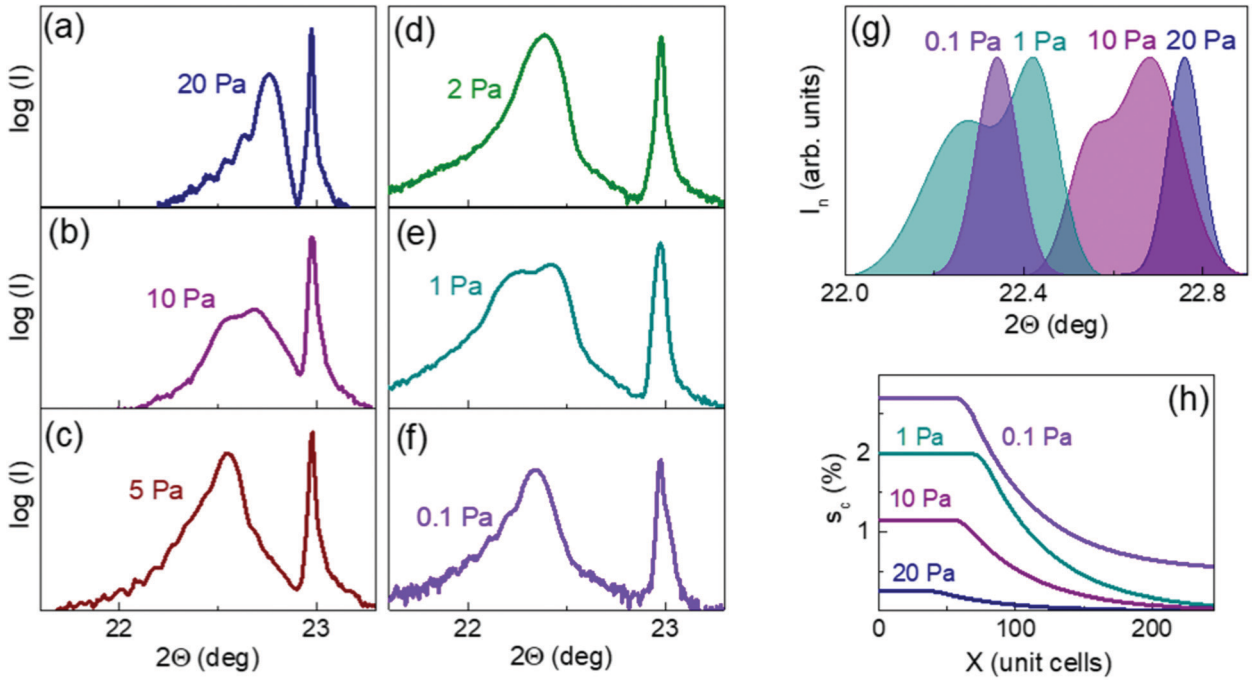

Fig. 2 (a–g) XRD Θ–2Θ scans around the (001) perovskite diffractions in the NNO/LSAT films deposited at different oxygen pressures. Sharp peaks are from the LSAT substrates in (a–f). The intensity is normalized in (g). (h) Model strain profiles for the peaks in (g): out-of-plane strain s_c as a function of the distance x from the film-substrate boundary.

to that in the substrate. The diffraction peaks from the films are broad [Fig. 2(a–g) and ESI† Fig. S2 and S3] and indicate a distribution of strain across the thickness.[11,33,34] The shapes, widths, and positions of the peaks vary with oxygen pressure in a complex manner. This behavior is clearly illustrated in Fig. 2(g).

The broad (001) peaks [Fig. 2(g)] generally agree with the expected presence of strain profiles, *i.e.*, the out-of-plane strain s_c is a function of distance x from the film/substrate boundary. However, it is impossible to precisely quantify the profiles $s_c(x)$ from XRD data because of the lack of relevant algorithms and software. Here, we applied a converse approach. We simulated the intensity for the (001) peaks assuming different model profiles as inputs. Diffraction intensities along the [001] reciprocal lattice directions were calculated using kinematic theory and varying sets of out-of-plane lattice parameters following the assumed strain profiles.[35] Stacks of alternating [AO] and [BO_2] planes were considered. The total thickness of each stack was 250 unit cells. The maximal strain was varied from 0.5 to 3%, the critical thickness ranged from 40 to 100 unit cells, and the relaxation was approximated by an exponential decay of strain. The simulations revealed sophisticated shapes of the intensity peaks. Although there were no straightforward connections of the shapes to the critical thickness, maximal strain, or inhomogeneous strain, we found important trends [ESI† Fig. S4], allowing for a semi-quantitative interpretation of the experimental data.

The measured peaks in Fig. 2(g) are consistent with the model profiles in Fig. 2(h). The maximal strain was estimated by fitting the (001) Θ–2Θ peaks as comprising two pseudo-Voigt peaks [ESI† Fig. S5]. The critical thickness was established based on the simulated intensities.

The obtained results imply tendencies for the critical thickness and maximal strain to grow with decreasing oxygen pressure. These observations prove the suggested elastic effects of the aligned oxygen vacancy dipoles. The presence of long relaxation "tails" in the profiles $s_c(x)$ is also akin to the expected spatial distribution of the aligned dipoles.

The maximal out-of-plane lattice parameter c, determined from the Θ–2Θ scans [ESI† Fig. S5], and average in-plane lattice parameter a, determined from the reciprocal space maps [ESI† Fig. S3], are plotted as a function of oxygen pressure in Fig. 3(a), where the out-of-plane strain is also shown. For the highest used pressure of 20 Pa, the measured out-of-plane strain s_c is less than 0.3%. With decreasing pressure, the parameter c heavily grows so that the strain s_c reaches $\sim$2.6% at 0.1 Pa. We considered two scenarios to analyze such a massive, nearly 10-fold increase in strain: conventional isotropic chemical expansion and peculiar anisotropic chemical expansion. Because both the chemical strain and misfit strain are present in the films, we assumed a chemically strained free-standing material, which is then subjected to substrate-controlled stress for each film. Importantly, whereas isotropic chemical expansion can result from isotropic dipoles of cationic vacancies and/or random orientation of anisotropic dipoles of oxygen vacancies, only aligned anisotropic dipoles of oxygen vacancies can produce anisotropic chemical expansion. We extracted the lattice parameters, chemical strain, and volumetric chemical expansion of the unstressed film material considering coherent near-surface fractions of the films, with the maximal

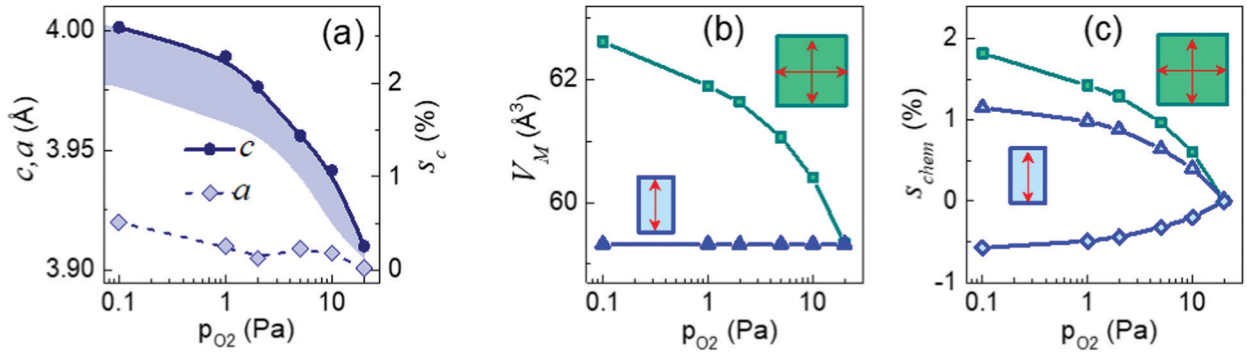

Fig. 3 (a) The maximal out-of-plane lattice parameter c and strain s_c (solid circles) as a function of oxygen pressure in the NNO/LSAT films. Diamonds show in-plane parameters a. (b) Unit-cell volume of the unstressed film material for the isotropic case (upper curve, illustrated by large squares) and anisotropic case (lower curve, illustrated by small rectangles). (c) Chemical strain in the unstressed film material: tensile strain for the isotropic case (squares) and tensile out-of-plane (triangles) and compressive in-plane (diamonds) strains for the anisotropic case.

out-of-plane parameters c and the in-plane parameters a = 3.868 Å equal to that of the LSAT substrate [ESI† "Epitaxy"]. The details of the procedure can be also found elsewhere.[22,36]

In the isotropic case, the material's unit-cell volume expands by nearly 6%, and the extracted chemical strain reaches 2% [Fig. 3(b and c)]. This huge chemical expansion alludes to nonsensical concentrations of cationic or random oxygen vacancies.[27,29] Furthermore, isotropic chemical expansion connotes an increase in the film-substrate in-plane misfit with decreasing pressure [ESI† Fig. S6]. This behavior should have led to efficient strain relaxation and, hence, to a chemically enlarged in-plane parameter $a \approx 3.98$ Å, which is in striking conflict with the experimental observations.

In the anisotropic case with the volumetric chemical expansion set to zero [Fig. 3(b)], the chemical strain is tensile up to ~1% in the out-of-plane direction and compressive in-plane [Fig. 3(c)]. Assuming $D_1 \approx 5$ eV and $c_{11} \approx 400$ GPa,[27,32] the corresponding concentration of the out-of-plane aligned oxygen vacancy dipoles may be up to $N \approx 5 \times 10^{27}$ m^{-3}, or ~6 at %, which is realistic. Notably, anisotropic chemical expansion facilitates coherent growth by diminishing the in-plane misfit [ESI† Fig. S6]. This behavior perfectly conforms with the enlarged critical thickness.

The experimental observations in the NNO/LSAT films validate the suggested increase in the critical thickness, above-misfit anisotropic strain, and large inhomogeneous strain in oxygen-deficient films. Furthermore, the analysis reveals that the chemical strain is anisotropic, which proves the suggested dipolar alignment.

Crossover from aligned to random dipoles in KNNO/STO films

The concentration N of the aligned oxygen vacancy dipoles is upper-limited by the concentration of oxygen vacancies but is not necessarily equal to that and can be smaller. Both random and aligned dipoles can be present in oxygen-deficient films. Then, the dominating anisotropic or isotropic chemical expansion is regulated by strain. Here, we demonstrate indications of such a strain-dependent crossover from the aligned to a random dipolar arrangement in KNNO/STO films.

The theoretical biaxial in-plane misfit strain is compressive [$s_a \approx -2.3\%$] for a cubic KNNO ($a_0 \approx 3.995$ Å)[37,38] on STO at the growth temperature. The room temperature lattice parameter of a pseudocubic perovskite cell of KNNO is $a_{0KNNO} \approx 3.984$ Å.[38] For the elastic constants of a model cubic KNNO as a mixture of $KNbO_3$ and $NaNbO_3$,[32] the room-temperature theoretical in-plane strain is [$s_a \approx -1.9\%$] and leads to the out-of-plane strain and lattice parameter [$s_c \approx 0.8\%$] and [$c \approx 4.016$ Å], respectively.

The room-temperature XRD Θ–2Θ scans and reciprocal space maps [ESI† Fig. S7–S10] indicated that the crystal structure of the KNNO/STO films could be treated as pseudocubic perovskite. In the films, the (00l) planes are parallel to the substrate (001) surface, and the [100] directions are parallel to those in the substrates. The positions and shapes of the diffraction peaks vary with oxygen pressure. This behavior is depicted using the normalized intensity of the (001) Θ–2Θ peaks [Fig. 4(a and b)]. The lattice parameters extracted from the XRD data are displayed as a function of the oxygen pressure in Fig. 4(c).

The XRD data signify that in the 20-Pa film of KNNO, the misfit strain is fully relaxed, and the out-of-plane lattice parameter shrinks due to thermal strain, similar to the previously demonstrated behavior of $BaTiO_3$ films.[39,40] Relaxation is as expected for stoichiometric KNNO/STO. The films deposited at lower pressures of 5–10 Pa contain strained fractions, where the parameter [$c \approx 4.06$ Å] exceeds the maximal theoretical value [Fig. 4(c)]. These observations are entirely in agreement with the misfit-stimulated dipolar alignment and consequent enlargement of the critical thickness and out-of-plane strain.

Upon further lowering the oxygen pressure, the vacancy concentration becomes larger, resulting in a significant fraction of random dipoles. Such dipoles produce isotropic chemical expansion of unstressed film materials. The film-substrate misfit for the expanded material rises and likely relaxes within a few nanometers at the film-substrate interface. The relaxation of the large effective misfit strain eradicates the driving force for dipolar alignment. Consequently, a transition from the dominating anisotropic expansion to a prevailing

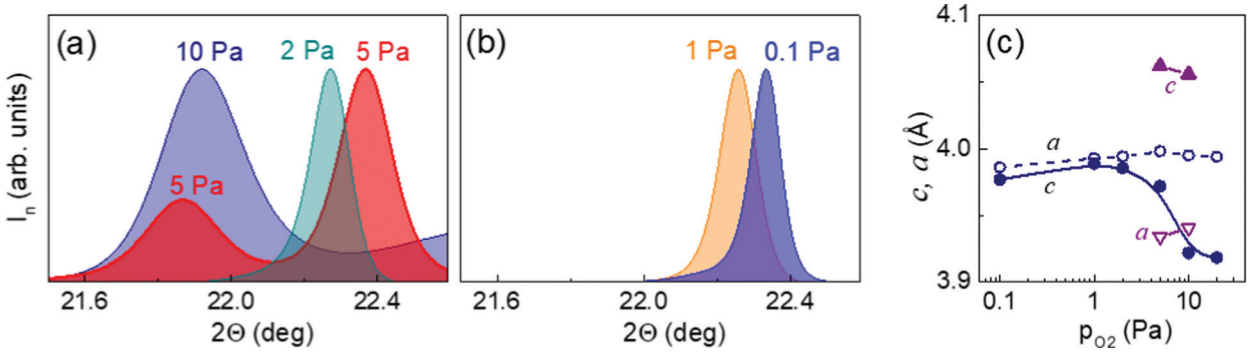

Fig. 4 (a and b) XRD Θ–2Θ scans around the (001) perovskite diffractions in the KNNO/STO films deposited at different oxygen pressures. The intensity is normalized. (c) The out-of-plane (solid symbols) and in-plane (open symbols) lattice parameters. Triangles show parameters in the strained fractions.

isotropic expansion can occur at low pressures. The suggested transition is corroborated by the crystal structure of the KNNO films deposited at 0.1–2 Pa. The out-of-plane lattice parameters are smaller in these films than in the strained fractions at 5–10 Pa [Fig. 4(c)]. Concurrently, noticeably narrower diffraction peaks substantiate a more pronounced relaxation of the misfit strain at lower pressures [Fig. 4(b)]. These characteristics point to a weaker dipolar alignment or an increased fraction of random dipoles occurring at 0.1–2 Pa. Assuming a hypothetical stable perovskite cell in the presence of a high concentration of random oxygen vacancy dipoles, the out-of-plane lattice parameter may further decrease at still lower pressures. Interestingly, such a decrease was previously experimentally observed in thin films of $BaTiO_3$.[41,42]

Reproducibility: BSTO/STO and BSTO/LSAT

The experimental verification of the suggested elastic effects was cross-checked by examining epitaxial BSTO films on compressive STO and LSAT substrates. The theoretical room-temperature in-plane misfit strain and the corresponding out-of-plane strain are [s_a = −1.3%] and [s_c = 1.1%] for BSTO/STO and [s_a = −2.3%] and [s_c = 2.0%] for BSTO/LSAT, respectively. Similar to the NNO/LSAT and KNNO/STO films, the BSTO films also grew with the (00l) planes parallel to the (001) surfaces of the substrates and with the [100] directions parallel to those in the substrates [ESI† Fig. S11–S15]. The diffraction peaks from the films are broad and altered with oxygen pressure, as summarized in Fig. 5(a and b). The maximal out-of-plane lattice parameter c and strain s_c significantly increase

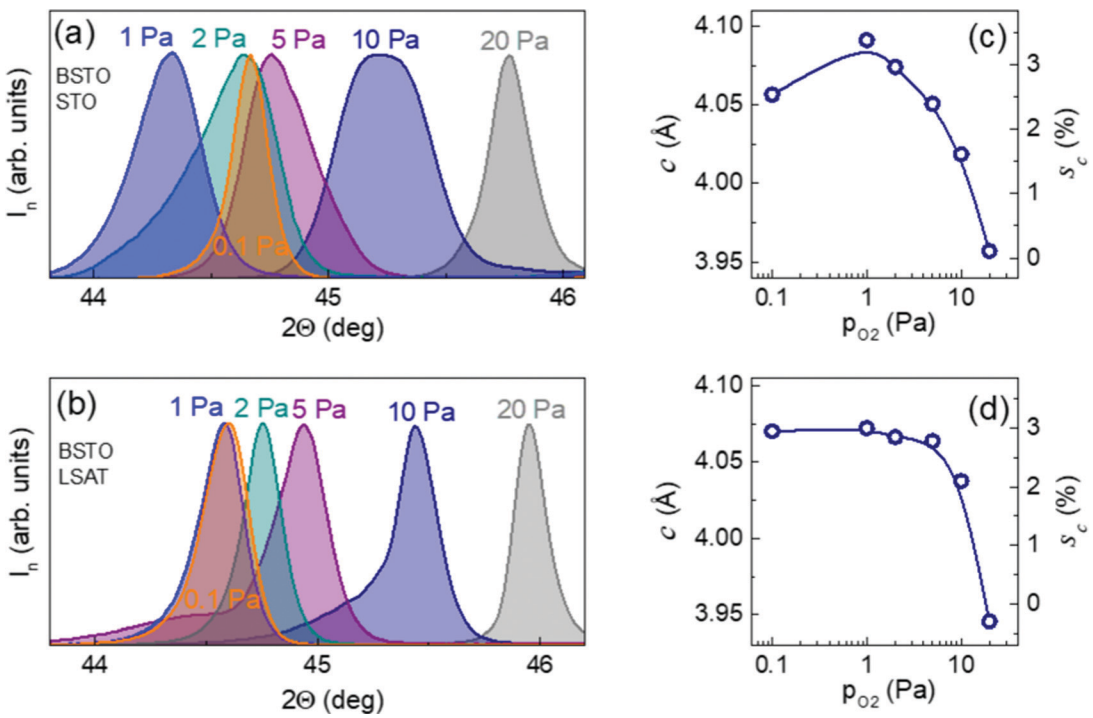

Fig. 5 (a and b) XRD Θ-2Θ scans around the (002) perovskite diffractions in the (a) BSTO/STO and (b) BSTO/LSAT films deposited at different oxygen pressures. The intensity is normalized. (c and d) The out-of-plane lattice parameters in the (a) BSTO/STO and (b) BSTO/LSAT films.

with decreasing pressure [Fig. 5(c and d)]. The measured strain s_c is up to 3% and exceeds the theoretical values for misfit strain. The shapes of the diffraction peaks indicate the presence of substantial inhomogeneous strain, which is also similar to the observations in NNO and KNNO and in accordance with the suggested behavior.

Discussion

The presented considerations and experimental observations demonstrate phenomenal elastic effects caused by the interactions of oxygen vacancies with misfit strain in perovskite oxide films. The key factor for these effects is an anisotropic elastic dipole tensor, characteristic of oxygen vacancies in perovskite oxides. The underlying process is a strain-stimulated crystallographic alignment of the vacancy dipoles. Currently, elastic dipoles of oxygen vacancies are not explicitly known, and elasticity theory for epitaxial films containing such dipoles has not yet been developed. However, the spectacular strength of the observed effects justifies the qualitative initial assessment.

A modified interaction between the B-site cations in the presence of an oxygen vacancy between them is a starting point to comprehend anisotropic vacancy dipoles. However, lattice distortions around oxygen vacancies involve all neighboring ions and may extend over a few unit cells. In a simplified notion of the B–Vo–B distortion, the main dipolar component D_1 alters with the charge state of the defect. Component D_1 can vary with the nominal charge of B cations, which commonly ranges from +3 to +5 in perovskite oxides, and/or with the charge of oxygen vacancies, which can be neutral, single charged, or doubly charged. Because minimization of elastic energy may promote not only strain-dependent preferable orientation of D_1 but also the maximal magnitude of D_1, it is possible that the macroscopic elastic energy of the strained film may control the vacancy charge: an elasto-electronic effect never considered before. Conversely, trapping electrons at V_O may principally reduce D_1 and thus lead to structural instability at sufficiently high concentrations of available electrons. We believe that this mechanism is responsible for the rapid degradation of strained oxygen-deficient films in transmission electron microscopy (which prevents cross-sectional examination of strain).

In polar perovskites, elastic dipoles of oxygen vacancies are intrinsically connected with electrical polarization. The corresponding additional electrostatic contribution to elastic vacancy-strain interactions may result in a combination of associated phenomena beyond purely elastic phenomena. For instance, misfit-driven alignment of vacancy dipoles in epitaxial films can produce an internal electric field therein. Experimental indications of a vacancy-related in-built field were detected in oxygen-deficient epitaxial films of $BaTiO_3$.[40,42]

Interactions of oxygen vacancies with misfit strain can lead to unusual elastic and electronic properties of epitaxial films of perovskite oxides. Because an external electric field or mechanical stress can alter the lattice strain and hence vacancy-strain interactions, unprecedented functional responses may arise in oxygen-deficient films. Likewise, vacancy-strain interactions may also affect the responses of many bulk perovskite oxides subjected to an external electric field or stress. Because anisotropic elastic dipole tensors may be associated with oxygen vacancies in perovskites and other metal oxides,[43–46] the demonstrated phenomena may have broad ubiquity. To predict multiple potential implications of macroscopic effects of vacancy-strain interactions, explicit knowledge of the atomic-level nature and macroscopic-level parameters of oxygen vacancies, as well as appropriate elasticity theory, are mandatory.

Conclusions

In epitaxial perovskite oxide films, interactions of oxygen vacancy dipoles with misfit strain were suggested to determine dipolar alignment and to thus lead to enlarged above-misfit strain and enhanced inhomogeneous strain. By varying the compressive misfit and oxygen content in thin films of niobate and titanate ferroelectrics, it was experimentally demonstrated that compared to stoichiometric films, the lattice strain is dramatically enhanced in the presence of oxygen vacancies, in agreement with the suggested effects. Analyses of oxygen-deficient films revealed anisotropy of the chemical strain, which confirmed the dipolar alignment. Furthermore, a non-monotonic dependence of lattice strain on the oxygen content was experimentally detected, in accordance with the expected coexistence of aligned and random dipolar arrangements. It was anticipated that the revealed remarkably strong elastic effects of oxygen vacancies can be essential for controlling strain in epitaxial films of a very broad range of functional perovskite oxides.

Author contributions

M. T.: conceptualization; funding acquisition; investigation; methodology; supervision; writing – original draft; writing – review & editing. J. L.: investigation; methodology. O. P.: investigation. T. K.: investigation. A. D.: funding acquisition.

Conflicts of interest

There are no conflicts to declare.

Acknowledgements

The authors acknowledge support from the European Structural and Investment Funds and the Ministry of Education, Youth and Sports of the Czech Republic through Programme "Research, Development and Education" (Project No. SOLID21 – CZ.02.1.01/0.0/0.0/16_019/0000760) and the Czech Science Foundation (Grant No. 22-10832S).

References

1 *Epitaxial Growth of Complex Metal Oxides*, ed. G. Koster, M. Huijben and G. Rijnders, Woodhead Publishing, Oxford, 2015.

2 J. L. MacManus-Driscoll, M. P. Wells, C. Yun, J.-W. Lee, C.-B. Eom and D. G. Schlom, *APL Mater.*, 2020, **8**, 040904.
3 N. A. Pertsev, A. G. Zembilgotov and A. K. Tagantsev, *Phys. Rev. Lett.*, 1998, **80**, 1988.
4 D. G. Schlom, L.-Q. Chen, C.-B. Eom, K. M. Rabe, S. K. Streiffer and J.-M. Triscone, *Annu. Rev. Mater. Res.*, 2007, **37**, 589.
5 J. Li, Z. Shan and E. Ma, *MRS Bull.*, 2014, **39**, 108.
6 B. Yildiz, *MRS Bull.*, 2014, **39**, 147.
7 D. G. Schlom, L.-Q. Chen, C. J. Fennie, V. Gopalan, D. A. Muller, X. Pan, R. Ramesh and R. Uecker, *MRS Bull.*, 2014, **39**, 118.
8 Z. Feng, N. Charles, X. R. Wang, D. Lee, K. A. Stoerzinger, S. Muy, R. R. Rao, D. Lee, R. Jacobs, D. Morgan and Y. Shao-Horn, *Mater. Today*, 2019, **31**, 100.
9 R. Ramesh and D. G. Schlom, *Nat. Rev. Mater.*, 2019, **4**, 257.
10 M. Ohring, *Materials Science of Thin Films*, Academic Press, San Diego, 2nd edn, 2002.
11 G. Catalan, B. Noheda, J. McAneney, L. J. Sinnamon and J. M. Gregg, *Phys. Rev. B: Condens. Matter Mater. Phys.*, 2005, **72**, 020102(R).
12 G. Catalan, A. Lubk, A. H. G. Vlooswijk, E. Snoeck, C. Magen, A. Janssens, G. Rispens, G. Rijnders, D. H. A. Blank and B. Noheda, *Nat. Mater.*, 2011, **10**, 963.
13 P. Zubko, G. Catalan and A. K. Tagantsev, *Annu. Rev. Mater. Res.*, 2013, **43**, 387.
14 A. N. Morozovska, E. A. Eliseev, C. M. Scherbakov and Y. M. Vysochanskii, *Phys. Rev. B*, 2016, **94**, 174112.
15 J. Zhang, C. Ji, Y. Shangguan, B. Guo, J. Wang, F. Huang, X. Lu and J. Zhu, *Phys. Rev. B*, 2018, **98**, 195133.
16 D. Sando, F. Appert, S. R. Burns, Q. Zhang, Y. Gallais, A. Sacuto, M. Cazayous, V. Garcia, S. Fusil, C. Carrétéro, J. M. Le Breton, A. Barthélémy, M. Bibes, J. Juraszek and V. Nagarajan, *Phys. Rev. Mater.*, 2019, **3**, 104404.
17 U. Aschauer, R. Pfenninger, S. M. Selbach, T. Grande and N. A. Spaldin, *Phys. Rev. B: Condens. Matter Mater. Phys.*, 2013, **88**, 054111.
18 U. Aschauer and N. A. Spaldin, *Appl. Phys. Lett.*, 2016, **109**, 031901.
19 J. Xi, H. Xu, Y. Zhang and W. J. Weber, *Phys. Chem. Chem. Phys.*, 2017, **19**, 6264.
20 M. Kotiuga, Z. Zhang, J. Li, F. Rodolakis, H. Zhou, R. Sutarto, F. He, Q. Wang, Y. Sun, Y. Wang, N. A. Aghamiri, S. B. Hancock, L. P. Rokhinson, D. P. Landau, Y. Abate, J. W. Freeland, R. Comin, S. Ramanathan and K. M. Rabe, *Proc. Natl. Acad. Sci. U. S. A.*, 2019, **116**, 21992.
21 T. H. Kim, T. H. Kim, T. R. Paudel, R. J. Green, K. Song, H.-S. Lee, S.-Y. Choi, J. Irwin, B. Noesges, L. J. Brillson, M. S. Rzchowski, G. A. Sawatzky, E. Y. Tsymbal and C. B. Eom, *Phys. Rev. B*, 2020, **101**, 121105(R).
22 M. Tyunina, L. L. Rusevich, E. A. Kotomin, O. Pacherova, T. Kocourek and A. Dejneka, *J. Mater. Chem. C*, 2021, **9**, 1693.
23 L. L. Rusevich, E. A. Kotomin, G. Zvejnieks and A. I. Popov, *Low Temp. Phys.*, 2020, **46**, 1185.
24 Y. F. Zhukovskii, E. A. Kotomin, S. Piskunov and D. E. Ellis, *Solid State Commun.*, 2009, **149**, 1359.
25 P. G. Sundell, M. E. Björketun and G. Wahnström, *Phys. Rev. B: Condens. Matter Mater. Phys.*, 2006, **73**, 104112.
26 C. Ricca, I. Timrov, M. Cococcioni, N. Marzari and U. Aschauer, *Phys. Rev. Res.*, 2020, **2**, 023313.
27 D. A. Freedman, D. Roundy and T. A. Arias, *Phys. Rev. B: Condens. Matter Mater. Phys.*, 2009, **80**, 064108.
28 E. Clouet, C. Varvenne and T. Jourdan, *Comput. Mater. Sci.*, 2018, **147**, 49.
29 E. J. Granhed, A. Lindman, C. Eklof-Osterberg, M. Karlsson, S. F. Parker and G. Wahnstrom, *J. Mater. Chem. A*, 2019, **7**, 16211.
30 T. Yamada, B. Wylie-van Eerd, O. Sakata, A. K. Tagantsev, H. Morioka, Y. Ehara, S. Yasui, H. Funakubo, T. Nagasaki and H. J. Trodahl, *Phys. Rev. B: Condens. Matter Mater. Phys.*, 2015, **91**, 214101.
31 I. Tomeno, Y. Tsunoda, K. Oka, M. Matsuura and M. Nishi, *Phys. Rev. B: Condens. Matter Mater. Phys.*, 2009, **80**, 104101.
32 A. Jain, S. P. Ong, G. Hautier, W. Chen, W. D. Richards, S. Dacek, S. Cholia, D. Gunter, D. Skinner, G. Ceder and K. A. Persson, *APL Mater.*, 2013, **1**, 011002.
33 D. Sando, M. Han, V. Govinden, O. Paull, F. Appert, C. Carrétéro, J. Fischer, A. Barthélémy, M. Bibes, V. Garcia, S. Fusil, B. Dkhil, J. Juraszek, Y. Zhu, X. Ma and V. Nagarajan, *Adv. Funct. Mater.*, 2020, **30**, 2000343.
34 P. Yudin, J. Duchon, O. Pacherova, M. Klementova, T. Kocourek, A. Dejneka and M. Tyunina, *Phys. Rev. Res.*, 2021, **3**, 033213.
35 I. Jaakola, J. Levoska and M. Tyunina, *J. Appl. Phys.*, 2007, **102**, 014108.
36 M. Tyunina, O. Pacherova, T. Kocourek and A. Dejneka, *Sci. Rep.*, 2021, **11**, 15247.
37 D. W. Baker, P. A. Thomas, N. Zhang and A. M. Glazer, *Appl. Phys. Lett.*, 2009, **95**, 091903.
38 J. Tellier, B. Malic, B. Dkhil, D. Jenko, J. Cilensek and M. Kosec, *Solid State Sci.*, 2009, **11**, 320.
39 M. Tyunina, O. Pacherova, J. Peräntie, M. Savinov, M. Jelinek, H. Jantunen and A. Dejneka, *Sci. Rep.*, 2019, **9**, 3677.
40 M. Tyunina, J. Peräntie, T. Kocourek, S. Saukko, H. Jantunen, M. Jelinek and A. Dejneka, *Phys. Rev. Res.*, 2020, **2**, 023056.
41 M. Li, J. Zhou, X. Jing, M. Zeng, S. Wu, J. Gao, Z. Zhang, X. Gao, X. Lu, J.-M. Liu and M. Alexe, *Adv. Electron. Mater.*, 2015, **1**, 1500069.
42 M. Tyunina, O. Vetokhina, N. Nepomniashchaia, O. Pacherova, S. Cichon, T. Kocourek, M. Jelinek and A. Dejneka, *APL Mater.*, 2020, **8**, 071107.
43 A. Janotti, J. B. Varley, P. Rinke, N. Umezawa, G. Kresse and C. G. Van de Walle, *Phys. Rev. B: Condens. Matter Mater. Phys.*, 2010, **81**, 085212.
44 A. Janotti and C. G. Van de Walle, *Appl. Phys. Lett.*, 2005, **87**, 122102.
45 D. Gryaznov, E. Blokhin, A. Sorokine, E. A. Kotomin, R. A. Evarestov, A. Bussmann-Holder and J. Maier, *J. Phys. Chem. C*, 2013, **117**, 13776.
46 I. Chatratin, F. P. Sabino, P. Reunchan, S. Limpijumnong, J. B. Varley, C. G. Van de Walle and A. Janotti, *Phys. Rev. Mater.*, 2019, **3**, 074604.